

Preparation and Properties of Transparent Conducting Oxide (TCOs) Thin Films: A Review

Raksha Dixit¹, Sushant Gupta¹, Praveen Kumar², Samiksha Sikarwar², B.C. Yadav*³

Ex-P.G. Student, Department of Applied Physics, School for Physical Sciences, Babasaheb Bhimrao Ambedkar

University, Lucknow, U.P., India¹

Ph.D. Student, Department of Applied Physics, School for Physical Sciences, Babasaheb Bhimrao Ambedkar

University, Lucknow, U.P., India²

Associate Professor, Department of Applied Physics, School for Physical Sciences, Babasaheb Bhimrao Ambedkar

University, Lucknow, U.P., India³

ABSTRACT: Present review reports the properties and applications of transparent conducting oxides (TCOs) thin films. Particular deposition techniques for TCO's manufacturing are important for several reasons as thickness uniformity and low production costs. In day to day life, transparent conducting oxide materials are used in various devices and mostly found in display technology, organic light-emitting-diodes, thin-film solar photovoltaics and smart windows. Also, they play a leading role in solid state gas sensors. Different types of oxides exhibit different response towards oxidising and reducing gases by the variation of their electrical properties. Detail discussion of electronic and optical properties of TCOs have also been carried out.

KEYWORDS: transparent conducting oxides; thin film; electrical and optical properties.

I. INTRODUCTION

In recent years, researchers have made quick and important developments in the arena of material science, especially in metal oxide semiconductor physics. Metal oxides are probably the most diverse, rich and multifunctional materials, with properties covering nearly all characteristics of materials science. Due to their unique characteristics, these metal oxides have found important applications in science e.g. ferri-, anti- and ferromagnetism, ferroelectricity, piezoelectricity, superconductivity, magnetoresistivity, photonics, catalysis, environmental engineering, etc. Oxides are also used in scientific applications in the production of microelectronic circuits [1, 2], sensors [3-12], piezoelectric devices [13], fuel cells [14], semiconductors [15-16], oxygen generators [17], organic synthetics [18-22], engineered ceramics [23], coatings against corrosion [24] and as catalysts [25-27]. All the metal oxides are the compound semiconductors consisting of two or more elements to show semiconducting properties. According to Wilson's model [28], the conductivity of metal oxides is the electronic type (ionic type is excluded) and is proportional to temperature. Also, it depends on the kind of impurities and their concentrations.

Some of the important metal oxide materials along with their chemical formulae, properties and applications have been summarised in Table 1. These metal oxides having structural features and oxygen deficiency responsible for creating many novel oxides possess unique electronic, optical, and chemical properties. However, nanosized metal oxides are particularly attractive to researchers due to their excellent properties [29-31]. These oxides are made into nanoparticles or thin/thick films to enhance their aspect ratio (surface area to volume ratio). Employing this high aspect ratio, nano-scale devices with greater performance and sensitivity can be fabricated [32].

International Journal of Innovative Research in Science, Engineering and Technology

(An ISO 3297: 2007 Certified Organization)

Website: www.ijirset.com

Vol. 6, Issue 2, February 2017

A wide variety of metal oxide nanoparticles have been manufactured exhausting alkali metal oxides, with molecular formula M_2O (M is Na or Li); and soluble metal salts (metal chlorides) in polar organic solutions, e.g., methanol and ethanol, at room temperature. The oxidation states of the metals in the synthesised metal oxides ranges.

Table 1: Properties and applications of some of the oxide materials

Oxides	Property	Applications
Al_2O_3 , CeO_2	Hardness	Abrasive
TiO_2 , CeO_2 , Fe_2O_3	Catalysts	Air and water purification
M^0/Al_2O_3 ($M^0 = Cu, Ag, Au, Pt, \text{ and } Pd$) $Ce_{1-x}M_xO_{2-\delta}$ ($M = Cu, Ag, Au, Pt, Pd, Rh,$ and Ru)	Redox catalyst	Three-way catalyst for automobile exhausts
$Ti_{1-x}M_xO_{2-\delta}$ ($M = Cu, Ag, Pt, Pd, Mn, Fe,$ Co, Ni and W)	Photocatalyst	Oxidation of organic matter
TiO_2 , ZnO	UV-Vis sunlight Absorbing	Photocatalyst, sunscreen, and paint
MTi/ZrO ₃ (M = Ca, Sr, Ba, and Pb); PZT	Dielectric	Sensors, MEMS
γ -Fe ₂ O ₃ , BaFe ₁₂ O ₁₉ , MFe ₂ O ₄	Superparamagnetic	Cancer detection and remediation, sensors and memory devices
TiO_2 , Fe_2O_3 , Cr_2O_3 M Al_2O_4 , MCr_2O_4 (M = transition metal ions) M/Al_2O_3 (M = Cr^{3+} , Co^{2+} , Ni^{2+}) M/ZrO_2 , RE/M:ZrSiO ₄ (M = Fe^{3+} , Mn^{2+} , V^{4+} ; RE = rare earth ion)	Colors	Ceramic pigments
Eu^{3+}/Y_2O_3 (red), Eu^{2+} , Tb^{3+} / Ba-hexa aluminate	Luminescence	Phosphors-CFL, colour TV picture tube
Al_2O_3 , ZrO_2 , ZTA, mullite, cordierite, tialite	Refractory	Toughened ceramics
MgO, CaO, and ZnO	Adsorbent	Defluoridation and chemical oxygen demand (COD) from paper mill effluents
YSZ(Y_2O_3 -ZrO ₂), Ni/YSZ, La(Sr)MO ₃ , M = Mn, Cr	Electrolyte, Anode/Cathode interconnect	Solid oxide fuel cell materials
Cu_2O	High absorption coefficient	Electrode material for solar cells
SnO_2	Transparent conductor	Electrode material for solar cells

from 1 to 6 and stay constant throughout the reactions and oxygen stoichiometry is maintained. These syntheses are based on a general ion reaction pathway during which the precipitate occurs when O^{2-} ions meet metal cations (M^{n+}) in anhydrous solution and the reaction equation is



Due to their unique properties of nanocrystalline oxide, researchers are highly interested towards them. Decreasing particle size results in the following remarkable properties:

- Catalytic along with photocatalytic activity is enhanced.

International Journal of Innovative Research in Science, Engineering and Technology

(An ISO 3297: 2007 Certified Organization)

Website: www.ijirset.com

Vol. 6, Issue 2, February 2017

- Mechanical reinforcement as in the case of carbon black in rubber is highly increased. Also, the hardness and strength of metals and alloys are enhanced.
- The electrical conductivity of ceramics as in CeO_2 is increased whereas it is decreased for metals like Cu, Ni, Fe, Co, and Cu alloys.
- Luminescence property of semiconductors is increased.
- The optical spectra of quantum dots have a higher shift towards the blue region.
- Superparamagnetic behaviour is also enhanced.
- High transmittance and conducting oxide (SnO_2).

However, the synthesis of dimension confined oxide nanomaterials is quite hard due to the agglomeration and nucleation during various synthesis steps. The precipitation of metal oxides solutions is less yielding than their sulphides or oxy salts counterparts. Reactions for the synthesis of metal oxides are based on two groups: one that produces an oxide directly [33-36] and the other is 'precursor' which is further subjected to various steps (calcination, dehydration, condensation, etc.) [37-38]. Maximum metal oxides are synthesised by the precipitation of respective metal hydroxides, carbonates, oxalates, and even nitrate products, monitored by successive calculations. High temperatures (calcination) or high pressures (hydrothermal treatment) are essential during the reactions, therefore, at such high-energy process, stoichiometry is challenging to monitor. Among them, thenon-aqueous sol-gel chemical route is the most promising [39] for providing high purity and homogeneity at low operating temperatures (200-300°C). Also, its aqueous counterpart for the synthesis of metal oxide materials in organic solvents provides some special features of better control over particle size, shape, crystallinity and surface properties [40].

II. SEMICONDUCTING MATERIALS

Chemical compounds of the type $\text{A}^{\text{III}}\text{B}^{\text{V}}$ cover a wide range of semiconductor materials, including arsenides, phosphides, antimonides, and nitrides in the form of GaAs, InAs, GaP, InP, InSb, AlN, and BN etc. These semiconductors obtained by different methods are used for the fabrication of single crystals from the liquid and gas phases, in inert chambers with high-strength and temperature. Impurities of group II and group IV elements are coated as p-type and n-type materials and are used in semiconductor lasers, light-emitting diodes, Gunn diodes, and photomultipliers, radiation detectors. The widely used $\text{A}^{\text{II}}\text{B}^{\text{VI}}$ type semiconductor materials are synthesised by chemical reactions in the gas phase and include ZnO, ZnS, CdS, CdSe, ZnSe, HgSe, CdTe, ZnTe and HgTe. These materials are characterised by resistivity, type of conductivity, energy band gap, carrier concentration, carrier mobility, the effective mass of the carriers, and carrier lifetime. Some characteristics like energy band gap and effective mass of the carriers are independent of the concentration of the chemical impurities and the degree of perfection of the crystal lattice whereas most of the properties are totally dependent on the concentration and nature of the chemical impurities and structural defects. Some of the physical properties of significant semiconductor materials are précised in Table 2. Semiconductor materials are employed either as bulk single crystals or as thin single-crystal and polycrystalline films on various substrates with a thickness of micron order in electronic devices, although their production is quite complicated. Such materials are immune towards the ambient environment and have certain stable electrical and physical characteristics. Among them, dislocation density and concentration of point defects are of much importance. High stability of such production requires constant temperature, the flow rate of the gas mixture, and period of the process, along with cleanliness. No more than four dust particles larger than 0.5μ per litre of air are allowed. Depending on the size of the single crystals and the type of the semiconductor material, the duration of single-crystal growth ranges from a few tens of minutes to several days. Control over certain parameters like chemical composition, type of conductivity, resistivity, carrier lifetime, carrier mobility and level of doping is quite essential and investigation of optical, spectroscopic, mass-spectrometric and activation are analysed by various sophisticated tools.

Importance and need of Nanomaterials

In recent years, nanoscience and nanotechnology have become one of the most interesting topics for researchers, for the control over structural, physical, chemical or biological properties of materials at the nanometer scale. Nanomaterials sometimes exhibit almost entirely different properties from their bulk counterpart due to their enhanced

International Journal of Innovative Research in Science, Engineering and Technology

(An ISO 3297: 2007 Certified Organization)

Website: www.ijirset.com

Vol. 6, Issue 2, February 2017

surface area. The surface atoms play a dominant role in the properties which involves the exchange of material with the surrounding at the interface; such as crystal growth, chemical reactivity and thermal conductivity.

Table 2: Some physical properties of important semiconductor materials

Nature of material	Material	Energy gap (eV)		Carrier mobility at 300 K (cm ² /volt-sec)		Crystal-structure type	Lattice constant (Å)	Melting point (°C)	Vapour pressure at melting pt. (atm)
		300 K	0 K	Electrons	Holes				
Element	C (diamond)	5.47	5.51	1,800	1,600	Diamond	3.56679	4027	10 ⁻⁹
A ^{IV} B ^{IV} compound	Ge	0.803	0.89	3,900	1,900	Diamond	5.65748	937	
	Si	1.12	1.16	1,500	600	Diamond	5.43086	1420	10 ⁻⁶
	a-Sn		-0.08			Diamond	6.4892		
	a-SiC	3	3.1	400	50	Zinc blende	4.358	3100	
A ^{III} B ^V Compound	AlSb	1.63	1.75	200	420	Zinc blende	6.1355	1050	<0.02
	BP	6				Zinc blende	4.538	>1300	>24
	GaN	3.5				Wurtzite	3.186 (a=axis) 5.176 (c=axis)	>1700	>200
	GaSb	0.67	0.80	4,000	1,400	Zinc blende	6.0955	706	<4 × 10 ⁻⁴
	GaAs	1.43	1.52	8,500	400	Zinc blende	5.6534	1239	1
	GaP	2.24	2.40	110	75	Zinc blende	5.4505	1467	35
	InSb	0.16	0.26	78,000	750	Zinc blende	6.4788	525	<10 ⁻⁵
	InAs	0.33	0.46	33,000	460	Zinc blende	6.0585	943	0.33
	InP	1.29	1.34	4,600	150	Zinc blende	5.8688	1060	25
A ^{II} B ^{VI} Compound	CdS	2.42	2.56	300	50	Wurtzite	4.16 (a=axis) 6.756 (c=axis)	1750	
	CdSe	1.7	1.85	800		Zinc blende	6.05	1258	
	ZnO	3.2		200		Cubic	4.58	1975	
	ZnS	3.6	3.7	165		Wurtzite	3.82 (a=axis)	1700	

At the nanometer scale, the number of atoms placed at the surface is considerably increased to the bulk scale. This plays the key role on the materials' properties. Assuming the particles to be spherical, the surface area to volume ratio can be given by $S/V = 3/r$, where r is the radius of the particle. Hence the decrease in particle's radius increases the surface to volume ratio (aspect ratio), e.g., a 1 cm³ of 1 nm sized particles would have an active surface area of about 100 m². At the nanoscale, a large fraction of the atoms is located in the grain boundaries, which is responsible for the excellent physical, mechanical, magnetic, electronic and biometric properties in comparison with coarse-grained/bulk (> 1 μm) materials. This is due to the fact that the grain boundary energy of nanocrystalline powders is larger than that of the fully equilibrated grain boundary. At this scale quantum confinement takes place, the electronic energy levels are discrete in nature instead of continuous. Hence, emissions from excited nanoparticles tend to show size-dependent vibrational frequencies: this property is useful in memory storage, sensor and electronics technologies [41]. Most semiconductor and metallic nanoparticles show strong particle size, shape and surrounding media dependent optical properties. The synthesis of nanomaterials is achieved essentially by the two approaches termed as "top-down" and "bottom-up" as described in Figure 1.

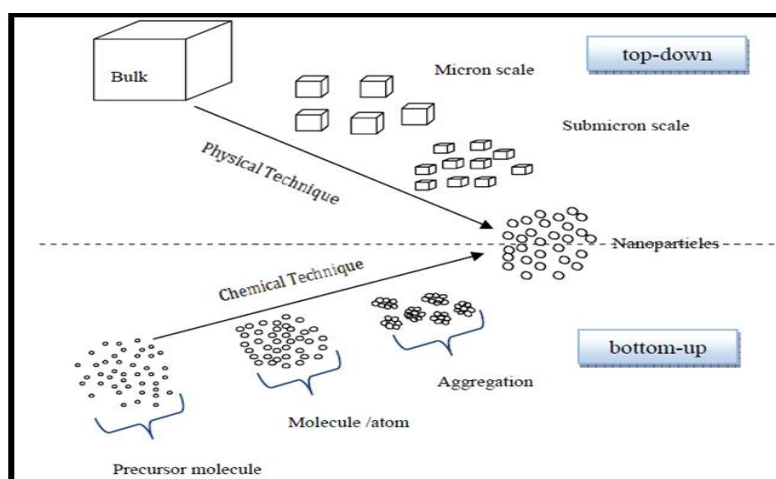


Figure.1 The two complementary approaches to nanoparticles synthesis.

In the top-down approach, carving down the size of materials from the bulk (macroscopic) to the nanometer scale takes place. This method usually involves the physical processes, or a blend of physical and/or chemical, electrical or thermal processes. The bottom-up approach involves assembling atom-by-atom or molecule-by-molecule into structures on the nanometer scale, where the characteristics vary relative to the number of constituent entities/grain size. Latter has a better control over all particles in the system. Micro-emulsion is an example of the bottom-up approach.

III.FUNDAMENTALS OF TRANSPARENT OXIDES (TCOS)

In our daily life,TCOs materials are used in numerous devices. These applications are mostly found in display technology, organic light-emitting-diodes (OLEDs), thin-film solar photovoltaics (PV) and smart windows. An arrangement of transparency and conduction can be attained in two classes of material. The first group is formed by extremely thin (~10 nm) metal films, especially Ag, Au or Cu. The luminous transmittance can go up to 50%, and even higher when the metal is sandwiched between anti-reflecting layers [42]. The conductivity is strongly thickness dependent, and therefore quite low for very thin films. The second class of materials consists of wide band gap semiconductors. As early as 1907s, the coexistence of electrical conductivity and optical transmittance was first observed in cadmium oxide. However, the technological advances in TCO have emerged only after the 1940s, as the potential applications in industry and research became evident. Years of extensive research finally led to SnO₂ doped In₂O₃ (ITO) with outstanding electrical and optical properties [43]. Hence at present, ITO is commonly used as transparent electrodes, especially in displays.

With the discovery of p-type TCOs, a new field in optoelectronics device technology has opened up. In contrast to passive electrodes, the use of transparent conductors as active components became possible. This has led to the innovative blue or ultra-violet (UV) LEDs [44-46]. Furthermore, it became possible to design all transparent devices. Although the fabrication of transparent circuits is nowadays limited to laboratory research [47], they are believed to find revolutionary applications in the next decades. However, appropriate p-type TCOs for this purpose is not available yet [48]. Moreover, most are far from suitable for processing on polymeric materials.

Understanding of the fundamental properties is important for an improvement of existing materials. Moreover, these insights are of great scientific importance for the design and synthesis of a new type of TCOs. The use of a deposition technique that allows indirect, but precise control of the fundamental properties can assist the research of high-performance TCOs on substrates. Limitations of TCOs have become more critical as passive and active devices based on these materials get more sophisticated. For example, as displays become larger and writing speeds get faster, it becomes increasingly important to decrease resistivity while the transparency is maintained. Simply increasing the

International Journal of Innovative Research in Science, Engineering and Technology

(An ISO 3297: 2007 Certified Organization)

Website: www.ijirset.com

Vol. 6, Issue 2, February 2017

thickness is not acceptable since the optical absorption will increase. A profound understanding of the fundamental aspects of transparent semiconductors is therefore required in order to improve either the properties of existing materials or design a new type of TCOs. These insights are of great scientific importance whether the realisation of high-performance TCOs on polymer substrates is possible. Reviews on TCOs concerning these issues have been reported earlier [49].

In next sections, we will discuss the electronic and optical properties of TCOs. Most of the considerations refer to indium oxide and indium tin oxide as an example, still, they hold for all other types of n-type transparent and conducting oxides. In most cases, this also holds for p-type semiconductors. The carrier density then refers to the hole concentration in the material. However, mobility and carrier density in p-type wide band gap semiconductors usually differ by a few orders of magnitude. The conduction mechanism can, therefore, be quite different.

Electrical Properties of TCOs

The conductivity (σ) is a product of the number of charge carriers (n) in a material with the mobility (μ) of these charge carriers and elementary electron charge (e). The resistivity (ρ) is defined as the inverse of the conductivity.

$$\sigma = e \cdot n \cdot \mu \dots\dots\dots (i)$$

For thin films of uniform thickness d , the electrical resistance is sometimes expressed as the sheet resistance ($R_s = \rho/d$). Other than the thickness, the sheet resistance is independent of the film dimensions. To increase the conductivity, the number of charge carriers should be increased by doping; and this can be done by substitutional doping, the creation of vacancies or implantation of interstitials. Also the valence of dopants or vacant sites, acceptor or donor states will induce p- or n-type conductivity.

Another way to increase the conductivity is to boost the mobility. However, the mobility is dependent on intrinsic scattering mechanisms, and can therefore not be monitored easily. In general, these mechanisms limit the mobility as the carrier density increases. As a result, the mobility is the most important parameter influencing the total conductivity. The presence of band gap, providing low absorption in the visible range, is an essential feature of TCOs. Metal oxide semiconductors having a minimum band gap of 3.0 eV meet this condition. The top of the valence band is mostly formed by the oxygen $2p$ bands, whereas the bottom of the conduction band is composed of a single and highly dispersed metals band. The O $2p$ orbitals are low in energy and it is therefore that a large band gap can be obtained in oxides. In intrinsic stoichiometric oxides, the coexistence of electrical conductivity beside visible transparency is not possible. However, substitutional doping by cationic donors or anion vacancies can create charge carriers, i.e. electrons. The donor (or acceptor) states alter the electronic band structure of the material. To improve donor density, the donor states combine with the conduction band at a definite critical density n_c , the magnitude of which can be obtained by Mott's criterion [50].

$$n_c^{-1/3} < c a_o^* \dots\dots\dots (ii)$$

Where a_o^* is the effective Bohr radius and c is a constant. The value of c is ≈ 0.25 . If this criterion is satisfied (i.e., if the density of electrons is sufficiently high) the material becomes conductive (metal) otherwise, it will be an insulator. The effective Bohr radius a_o^* is given by:

$$a_o^* = \frac{h^2 \epsilon_o \epsilon^m}{\pi e^2 m_c^*} \dots\dots\dots (iii)$$

Where ϵ^m is the static dielectric constant of the host lattice (8.9 for In_2O_3) [51], and m_c^* is the effective mass of the electrons in the conduction band. After comparing experimental data of several authors, Kostlin et al. calculated the effective mass of In_2O_3 to be about one-third of the electron rest mass; i.e. $m_c^* = 0.35 m_e$. Using these numbers, one can obtain $a_o^* \approx 1.3$ nm, and the critical density n_c is calculated as $6.4 \times 10^{18} \text{ cm}^{-3}$. Generally, the carrier density in TCOs is by far larger than this (up to 10^{21} cm^{-3} in ITO). Above this Mott critical density, free electron behaviour can be expected. The donor states have merged with the conduction band and the material is said to be degenerate. The Fermi energy E_F is obtained by the highest occupied state of the conduction band, and one can write:

International Journal of Innovative Research in Science, Engineering and Technology

(An ISO 3297: 2007 Certified Organization)

Website: www.ijirset.com

Vol. 6, Issue 2, February 2017

$$E_F = \frac{\hbar^2 k^2}{2 m_c^*} \dots\dots\dots(\text{iv})$$

The band structure of tin oxide is estimated by parabolic functions of k close to the band edges. The schematic representation in Figure 2 is valid for most binary metal oxide wide band gap semiconductors. The valence band maximum and conduction band minimum are both placed at k = 0, so the material is said to be a direct band semiconductor.

If optical transitions or carrier transport occur far from the conduction band bottom or valence band top, the shape of the bands is slightly distorted. This band distortion is caused by interactions with other bands and many-body effects. It is, therefore, hard to determine the effective mass theoretically in these regions, since this value is determined by the band curvature. For theoretical calculations on the band structure, non-parabolic effects should be taken into consideration [52].

Scattering Mechanism

As mentioned earlier, the conductivity of TCOs is reflected from the mobility that can be expressed as:

$$\mu = \frac{e \cdot \tau}{m^*} = \frac{e \cdot \lambda_{mfp}}{m^* \cdot v_F} \dots\dots\dots(\text{v})$$

The relaxation time τ is dependent on the drift velocity v_F and mean free path λ_{mfp} of the charge carriers. The factors are affected by the different scattering; lattice type, ionised impurity type, neutral impurity type, electron-electron type, electron-impurity type and grain boundary type^[51]. The total mobility can, therefore, be written as:

$$\frac{1}{\mu_{tot}} = \sum_i \frac{1}{\mu_i} \dots\dots\dots(\text{vi})$$

In crystalline TCOs, all scattering mechanisms have little effect, except the ionised impurity scattering. However, TCOs deposited at lower temperatures possess a lower crystalline nature, and high doping concentrations result in the formation of neutral complexes. In these cases, grain boundary and neutral impurity scattering should also be taken into consideration.

Ionized Impurity Scattering

The Coulomb interaction between the ionised (donor) impurities and the free electrons provide an intrinsic source of scattering to the doped material, and can, therefore, reduce the resistivity, in spite of neutral impurities, grain boundaries or structural disorder. The attainable resistivity due to ionised impurity scattering was first calculated by Brooks (1955), using the Born approximation band Thomas-Fermi screening. The theory assumes that the ionised impurities form a uniform background of immobile charges. The mobile charges (electrons or holes) provide screening. The relaxation time of an electron of wave vector k is then given by:

$$\frac{1}{\tau(k)} = \frac{N_i Z^2 e^4 m^*}{8\pi(\epsilon_o \epsilon_r)^2 \hbar^3 k^3} f(k) \dots\dots\dots(\text{vii})$$

Here is N_i the number of scattering centres per unit volume and Z the charge on the impurity, ϵ_o represents the permittivity of free space, whereas ϵ_r is the low-frequency relative permittivity. $f(k)$ is the screening function and is dependent on the Thomas-Fermi screening wave vector. A degenerate system requires only the scattering of electrons at the Fermi surface ($k = k_F$).

The upper limit of the mobility can now be expressed by:

$$\mu_{iis} = \frac{24\pi^3 (\epsilon_o \epsilon_r)^2 \hbar^3 n}{N_i Z^2 e^3 m^{*2}} \frac{1}{f(k_F)} \dots\dots\dots(\text{viii})$$

Later, Moore [52] corrected the Dingle's work based on second order terms in the Born approximation. This resulted in a slightly lower mobility limit. Pisarkiewicz et al. [53] applied corrections to this model by taking into

account the non-parabolic band shape. This caused a larger effect on the intrinsic limit. According to his approximation, the effective mass at the Fermi energy is dependent on the carrier concentration as;

$$m^* = m_o^* \sqrt{1 + 2C \frac{\hbar^2}{m_o^*} (3\pi^2 n)^{2/3}} \dots\dots\dots(ix)$$

Where C is a constant used to fit experimental data. Equations (vii) and (viii) can be used to calculate the intrinsic mobility limit in terms of carrier concentration n.

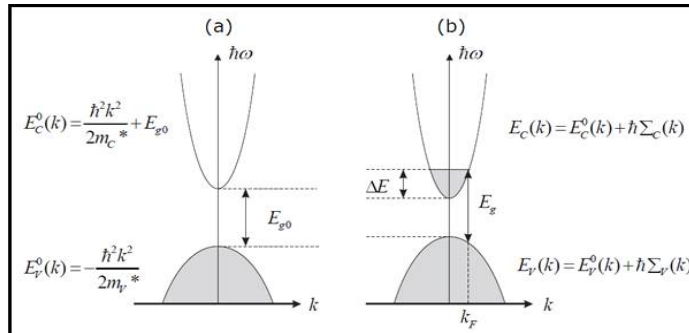
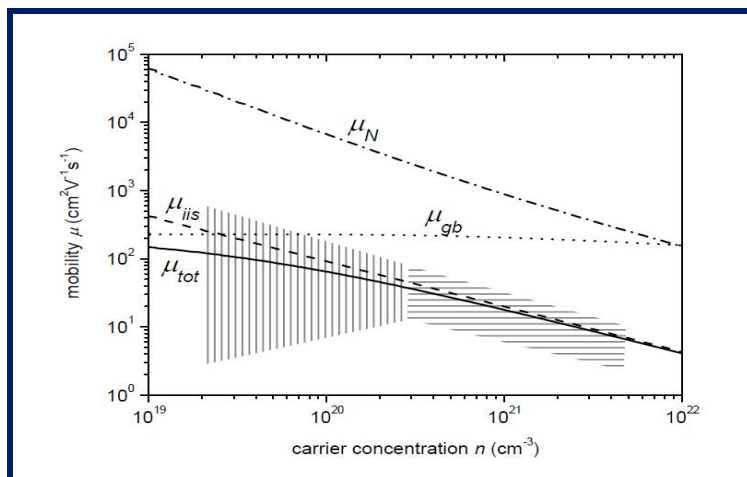


Figure 2: Schematic representation of the band structure of undoped (a) and doped (b) metal oxide wide band gap semiconductor.

Grain Boundary Scattering

The grain boundary, made of some atomic layers of disordered atoms, is a complicated structure. These incomplete atomic bonds make a large number of defects. Here charge carriers are trapped; i.e. immobilised. The traps become electrically charged, creating a potential energy barrier, reducing the mobility of free carriers from moving from one crystallite to the other. Seto [54] assumed a barrier with thickness d, which is considerably smaller than grain size L. Further the grain boundary contains Q_t traps per cubic centimetre located at energy E_t relative to the intrinsic Fermi level.

All charges in the region with thickness d around the grain boundary are supposed to be trapped and form a depletion layer. The grain boundary can be supposed of a potential barrier for electrons determined by its height E_b . The contribution μ_{gb} is thermally activated and can be explained by the Petritzrelation [55]:



International Journal of Innovative Research in Science, Engineering and Technology

(An ISO 3297: 2007 Certified Organization)

Website: www.ijirset.com

Vol. 6, Issue 2, February 2017

Figure 3: The upper limit of mobility (solid line) influenced by the effect of scattering on ionised impurities (dashed curve), grain boundaries (dotted curve) and neutral impurities (dash-dotted curve). μ_{iis} was calculated for double ionised donors (oxygen vacancies; $Ni \cdot Z^2 = 2n$) resulting in larger contribution.

$$\mu_{gb} = \mu_o \exp\left(-\frac{E_b}{k_b T}\right), \text{ with } \mu_o = \frac{L_q}{\sqrt{2\pi m^* k_b T}} \dots\dots\dots(x)$$

Where q is the charge of the trap, k_b is Boltzmann constant and T is the absolute temperature. The energy barrier height is:

$$E_b = \frac{q^2 Q_t^2}{8\epsilon_o \epsilon_r N_d}, \text{ with } N_d = n + \frac{Q_t}{d} \dots\dots\dots(xi)$$

N_d is the total number of ionised donors. Free fitting parameters are; the number of traps Q_t and barrier thickness d. This model was later applied to TCO materials [55], and data of polycrystalline ITO, F: SnO₂ [56] and ZnO [57] films was fitted to this relation. It has been shown that the energy barrier height is approximately 0.01 eV.

The grain boundary scattering is effective on the total mobility iff the grain size has the same order of dimensions as the mean free path of the charge carriers ($L \sim \lambda_{mfp}$). The mean free path can be calculated for known carrier density and mobility. Using a highly degenerate electron gas model the electron velocity V_F is:

$$V_F = (3\pi^2)^{1/3} (\hbar / m^*) n^{1/3} \dots\dots\dots(xii)$$

Substitution in equation (v) results in the following expression for the mean free path λ_{mfp} :

$$\lambda = V_F \tau = V_F \frac{m^* \mu}{e} = (3\pi^2)^{1/3} (\hbar \mu / e) n^{1/3} \dots\dots\dots(xiii)$$

Neutral Impurity Scattering

The solubility of dopants in oxide semiconductors can be quite high. The solid solubility limit of Sn in ITO, for instance, is found to be well over 60%. At high doping concentrations, an increasing amount of dopant material remains inactive, and can form a variety of neutral complexes. Therefore neutral impurity scattering might be taken into consideration. The contribution to the mobility μ_N is given by [58-59]

$$\mu_N = \frac{m^* e^3}{20\epsilon_o \epsilon_r \epsilon_N \hbar^3} \dots\dots\dots(xiv)$$

where μ_N is the concentration of neutral impurities and is obtained from the difference between measured carrier density and carrier concentration. The ionised impurity and grain boundary scattering, on the other hand, show a direct relation with the carrier concentration.

Intrinsic Conductivity Limit

According to the previous sections, the maximum conductivity of wide band gap semiconductors is restricted by the theoretical upper limit of mobility. This intrinsic mobility limit is dependent on carrier concentration for each scattering mechanism. Modelling the upper limit of separate or combined mechanisms for different TCOs materials has been reported frequently. In Figure 3 the upper of mobility was simulated for polycrystalline indium oxide with intermediate grain size (50 nm). The total mobility limit is determined by the contributions of the scattering mechanisms from relations (viii), (x) and (xi). The nonparabolicity of the conduction band has been taken into account in the calculations. It can be seen that the importance of electron scattering on neutral impurities has a negligible effect on the total mobility. A number of neutral impurities in relation (xi) were even overestimated since it was set to half the number of free carriers. The values for the mobility reported in the literature are all located in the marked areas of Figure 3. Best performing films are found in the region where the ionised impurity scattering is dominant (horizontal lines). If the grain size is small enough, TCOs thin films up to intermediate carrier density are affected by grain boundary scattering as well (vertical lines). Although most authors agree on the mobility limit due to ionised impurity scattering, the mobility due to grain boundary scattering is modelled differently in many cases. Apparently, the free parameters are used to fit the obtained data exactly, whereas in general, the average grain size is just a rough estimate.

International Journal of Innovative Research in Science, Engineering and Technology

(An ISO 3297: 2007 Certified Organization)

Website: www.ijirset.com

Vol. 6, Issue 2, February 2017

Therefore the influence of grain boundary scattering in TCOs is still under debate. However, it is commonly accepted that the mobility is only affected if the grain size is considerably small. And moreover, this effect is only noticeable up to intermediate carrier concentrations, as for high electron density the ionised impurity scattering dominates.

The effect of ionised impurities is dominant (horizontal lines) or grain boundaries can play a role (vertical lines). From Figure 4 it is evident that the structure of TCOs thin films affects the electrical properties continuing from single- to polycrystalline phase. As the grain size decreases further, the thin film is said to be nanocrystalline or even amorphous. Although the grain boundary density increases to infinity in the amorphous state, the mobility does not drop to zero e.g., in some amorphous oxide materials a reasonable mobility can be obtained, resulting in amorphous conductivity. In a most n-type transparent conductor, the bottom of the conduction band consists of a highly discrete single s-band. This elevated dispersion and s-type character consequence in a much uniform distribution of the electron charge density. The scattering of these states is relatively low and provides a large mobility. As mentioned earlier, a high mobility is critical in attaining a high conductivity. The mobility being proportional to the width of the conduction bands, a great overlap between the relevant orbitals is essential. The amount of this overlap is also of great importance in the case of polycrystalline or amorphous materials. A large overlap is rather insensible to the structural ill-orders of the amorphous state. The spatial spreading of the spherical s-orbitals should be large enough to create continuous conduction paths. In particular, for post-transition metal cations, a direct overlap between neighbouring metal s-orbitals is possible. The conduction paths become insensitive to the distorted metal-oxygen-metal bonds in amorphous materials as schematically illustrated in Figure 5. Therefore, the mobility in amorphous oxide semiconductors can be similar to the corresponding crystalline phase ($>10 \text{ cm}^2\text{s}^{-1}\text{V}^{-1}$).

Optical Properties

(i) Transparency

An important feature of TCOs is the existence of a transmission window covering a wide range of the visible spectrum. In literature, the optical transmission is defined as the ratio between incoming light intensity and transmitted intensity averaged over all values in between 400 nm and 700 nm. The typical spectral dependence of TCOs is schematically shown in Figure 5. The transmission window is defined by two regions where no light is transmitted due to different phenomena. At low wavelengths ($\lambda < \lambda_{\text{gap}}$) the absorption due to the fundamental band gap dominates. The photon energy in this near-and deep-UV part of the spectrum is high enough to equal the band gap energy (3-4 eV). This energy is absorbed and transformed to the band to band transitions, and no light is transmitted because of this quantum phenomenon. For longer wavelengths, in the (near) infrared (IR) part of the spectrum, no light is transmitted due to the plasma edge ($\lambda > \lambda_p$). Here the light is electronically reflected which can be best described by the classical Drude free-electron theory.

In the free electron model, the electrons may be thought of as plasma whose density is set into motion by the electric field component of the electromagnetic field. The plasma oscillates at a natural frequency ω_p , the resonance or plasma frequency. This frequency corresponds to the plasma wavelength λ_p and is of the order of 1-4 μm for TCOs. The interaction of free electrons with the electromagnetic field influences the relative permittivity ϵ of the material, which is expressed as a complex number:

$$\epsilon = (N - ik')^2 \dots\dots\dots(xv)$$

The real and imaginary part is the refractive index (N) and the extinction coefficient (k') respectively. These parameters determine the reflectance and absorbance of the material. Close to the plasma frequency the properties of the material changes drastically. In the infrared (IR) part of the spectrum, below this critical value ($\lambda > \lambda_p$) the imaginary part of the formula (xv) is large, and the penetrating wave drops off exponentially. The real part is negative, and the material has near unity reflectance. For $\omega > \omega_p$ (or $\lambda < \lambda_p$), the imaginary part tends to zero, and absorption is small. The refractive index is positive and almost constant with frequency according to:

$$N = \epsilon_{\infty}^{1/2} \sqrt{1 - (\omega_p / \omega)^2} \cong \sqrt{\epsilon_{\infty}} \dots\dots\dots(xvi)$$

Here ϵ_{∞} is the high-frequency permittivity. The TCOs behave like a dielectric and is transparent in the region for $\omega > \omega_p$. In this transparent regime the film is weakly absorbing ($k'^2 < N^2$) and the transmission can be expressed as [60]:

International Journal of Innovative Research in Science, Engineering and Technology

(An ISO 3297: 2007 Certified Organization)

Website: www.ijirset.com

Vol. 6, Issue 2, February 2017

$$T = (1 - R) \exp(-\alpha d) \dots \dots \dots (xvii)$$

R is the zero degree incidence reflectance, d is the film thickness and α is the absorption coefficient and is dependent on the wavelength according to:

$$\alpha = \frac{4\pi k'}{\lambda} \dots \dots \dots (xviii)$$

Close to λ_{gap} the reflectance is zero and the absorption coefficient as a function of wavelength can be obtained easily from the transmission curve. The following relation applies for directly allowed transitions:

$$\alpha \propto \sqrt{h\nu - E_g} \dots \dots \dots (xix)$$

where $h\nu$ is the photon energy. The band gap energy is calculated from the Tauc plot, α^2 versus the photon energy $h\nu$. If α^2 is extrapolated to the X-axis intersection ($\alpha^2 = 0$), formula (xix) implies that the photon energy equals the band gap energy ($h\nu \propto E_g$). This method is commonplace to extract band gap energies from transmission data.

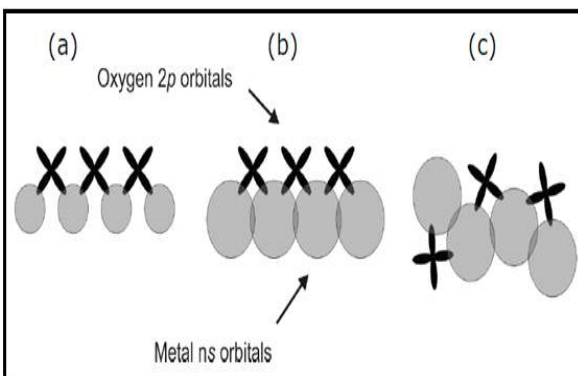


Figure 4: Schematic illustration of the electron density in the atomic orbitals responsible for the carrier transport paths in TCO (a), heavy metal cations in crystalline phase (b) and amorphous phase (c). In 'ns orbitals' the n denotes the principal quantum number.

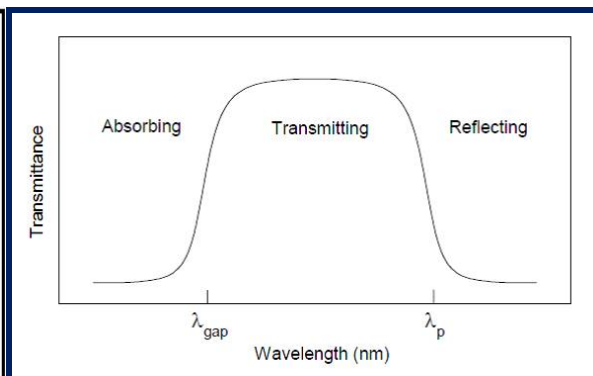


Figure 5: Spectral dependence of semiconducting transparent materials: λ_{gap} and λ_p are the wavelengths at which the band gap absorption and free electron plasma absorption takes place.

(ii) Correlation of Optical-Electrical Properties

The optical parameters of TCOs are influenced by the electrical properties of the material. The earlier mentioned plasma resonance frequency is not a fixed value but varies with the electron concentration. The plasma frequency in relation to the carrier concentration is expressed by:

$$\omega_p = \sqrt{\frac{n \cdot e^2}{\epsilon_o \epsilon_\infty m_c^*}} \dots \dots \dots (xx)$$

At this frequency, the dielectric-like visible transmittance equals the metallic-like IR reflectance ($T = R$).

Thus, IR reflectivity of the material can be adjusted, which is important for heat reflecting or low emissive window applications. For example, the plasma wavelength of ITO films can be tuned from 1.5 μm to 4 μm due to the carrier concentration by changing the composition and deposition parameters. The refractive index of commonly TCOs materials varies in between 1.7 and 2.1. Moreover, a large spread of the similar material is frequently reported. Main reason is that the refractive index is also dependent on the carrier concentration according to the equation given as under:

International Journal of Innovative Research in Science, Engineering and Technology

(An ISO 3297: 2007 Certified Organization)

Website: www.ijirset.com

Vol. 6, Issue 2, February 2017

$$N^2 = \epsilon_{opt} - \frac{4\pi ne^2}{m^* \omega^2} \dots\dots\dots(xxi)$$

Here ω is the frequency of incident light. Changing the refractive index is useful for waveguide applications e.g., in ITO this value can be tuned between 1.70 and 2.05 [61-62]. For heavily doped oxide semiconductors a gradual shift of the band gap towards higher energy as the electron density increases is generally observed [56]. This well-known effect is attributed to the Burstein-Moss shift (BM shift). In heavily doped semiconductors, the lowest states in the conduction band are blocked. Hence transition can only take place to energies above E_F (Figure 2), enlarging the effective optical gap. The energy gap between the top of the valence band and lowest empty state in the conduction band (both assumed parabolic) can be given by:

$$E_g = E_{go} = \Delta E_g^{BM} - \hbar \Sigma \dots\dots\dots(xxii)$$

In this formula E_{go} is the intrinsic band gap and the BM shift given by:

$$\Delta E_g^{B-M} = \frac{\hbar^2}{2m_{VC}^*} (3\pi^2 n)^{2/3} \dots\dots\dots(xxiii)$$

Here, the reduced effective mass of the electron carriers is given by:

$$\frac{1}{m_{VC}^*} = \frac{1}{m_c^*} = \frac{1}{m_v^*} \dots\dots\dots(xix)$$

Where m_c^* and m_v^* are the effective mass of the carriers in the conduction and valence band respectively.

Some n-type and p-type TCOs are described in Tables 3 and 4, respectively. The references in these tables are not selected on the best performance of the TCOs but are merely a selection of the vast amount of literature on these materials. It illustrates the diversity of materials and corresponding properties deposited by different deposition methods. Among these are chemical vapour deposition (CVD), sputtering techniques (DC, RF, Magnetron), evaporation (reactive, thermal or e-beam), spray pyrolysis and pulsed laser deposition (PLD). Particular deposition techniques for TCO's manufacturing are chosen for several reasons as thickness uniformity and low production cost. However, the electrical and optical performance is not directly related to the deposition method. They are more dependent on the intrinsic properties as structure, morphology and composition of the thin film. Each deposition method and conditions can influence the intrinsic behaviour differently. Although each technique has its own advantages or limitations, they are all capable of turning the intrinsic properties within a specific range in order to optimise the TCO's performance.

Coexistence of transparency and conductivity in semiconductors is possible if the band gap is large enough to avoid visible light absorption (~ 3 eV). This gap is situated in between parabolic O 2p and metal s bands, forming the valence and conduction band respectively. Intentional doping creates free carriers (electrons or holes) which are responsible for the conductivity. Electron densities are in general high for n-type TCOs (order 10^{20} cm^{-3}) resulting in degenerate electron systems. The electrical conductivity is dominated by scattering mechanisms, which are strongly related to the electron concentration. All electronic scattering contributions together influence the mobility and determine the upper limit of conductivity. For single-crystalline materials, the ionised impurity scattering is considered of great importance. Though, as the structural nature of the thin film decrease, the contribution of grain boundaries becomes ever more important in polycrystalline films. The transparency window for electromagnetic waves between UV and near-IR is typical for TCOs. This window is on the short wavelength side determined by the band gap and on the long wavelength side by the plasma frequency. Both values are dependent on the electron concentration, and can, therefore, be tuned to serve specific applications. The electrical conductivity of common n-type materials is around $10^{-4} \Omega\text{-cm}$, whereas the transmission can be as high as 90% in the visible regime. The conductivity of p-type TCOs is in general at least a factor of 1000 lower. Although the figure of merit is a measure of the TCO's electrical and optical performance, in practice the properties are tailored for the different applications. Many deposition methods can be used to grow TCOs and varying performances are reported. Each deposition method has its own influence on the intrinsic

International Journal of Innovative Research in Science, Engineering and Technology

(An ISO 3297: 2007 Certified Organization)

Website: www.ijirset.com

Vol. 6, Issue 2, February 2017

properties as thin film structure and composition. It is these properties and not the deposition method by itself determining the electrical and optical performance of the TCOs.

TCOs also play an important role in solid state gas sensors by exhibiting sensitivity towards gases in terms of changing electrical properties. The gas sensitivity of oxides is related to the surface chemical activity. The metal oxides provide strong and resourceful foundation materials in the fabrication of novel technologies such as superconducting electronics, microwave communications, ferroelectric memories, infrared detectors, magnetic sensors, transparent conducting coatings and gas sensors.

Table 3: Reported properties of n-type TCOs.

TCO	Deposition Method	ρ (Ωcm)	T^{II} %	FOM ($10^{-3}\Omega^{-1}$)	E_g (eV)	N	N (cm^{-3})	M ($\text{cm}^2/\text{s/V}$)	Ref.
SnO ₂	Sputtering	6.1×10^{-3}	95	56.4	4.13		1.3×10^{20}	7.7	63
SnO ₂ :F	Spray	5×10^{-4}	>80		4.41		4.6×10^{20}	28	64
SnO ₂ :Mo	Reactive ev.	3×10^{-3}	>85	>0.07	4.10		8.0×10^{20}	10	65
SnO ₂ :Sb	Spray	10^{-3}	85	19.6	3.75		7.0×10^{20}	10	66
Cd ₂ SnO ₄	Sputtering	5×10^{-4}	>80			2.05	5.0×10^{20}	40	67
In ₄ Sn ₃ O ₁₂	Sputtering	3.5×10^{-4}	>80		3.5	2.1	7.0×10^{20}	11.5	68
GaInO ₃	Sputtering	2.5×10^{-3}	90	14			4×10^{20}	10	69
ITO	e-beameva.	2.4×10^{-4}	90		3.85	2.0	8.0×10^{20}	30	70
ITO	CVD	1.7×10^{-4}	90	183	3.9		8.8×10^{20}	43	71
ITO	Sputtering	2.4×10^{-4}	95	70.4	4.0	2.0	1×10^{20}	12	72
ITO:F	R.F. Sputtering	6.7×10^{-4}	>80	3.5			6.0×10^{20}	16	73
ZnO	R.F. Reactive Sputtering	2×10^{-3}	>80	4			1.2×10^{20}	16	74
ZnO:Al	CVD	3.3×10^{-4}	85	49.2			8.0×10^{20}	35	75
ZnO:Ga	Sputtering	10^{-3}	>85		3.59		10×10^{20}	10	76
ZnO:In	Sputtering	2×10^{-2}	>80	3.29		1.85	7×10^{19}	1.9	77
Zn ₃ In ₂ O ₆	PLD	1.0×10^{-3}	85		3.4		4.0×10^{20}	20	78

Table 4: Reported properties of p-type TCOs

TCO	Deposition method	σ^{III} (Scm^{-1})	T %	E_g (eV)	S $\mu\text{V/K}$	E_a (eV)	n (cm^{-3})	μ ($\text{cm}^2/\text{s/V}$)	Ref.
CuAlO ₂	PLD	0.34	70	3.5	+214	0.22	2.7×10^{19}	0.13	79
SrCu ₂ O ₂	PLD	4.8×10^{-2}	75	3.3	+260	0.10	6.1×10^{17}	0.46	80
CuYO ₂ :Ca	Thermal evaporation	1.0	50	3.5	+275	0.13		>1.0	81
AgCoO ₂	Sputtering	0.2	50	4.15	+220	0.07			82
CuGaO ₂	PLD	6.3×10^{-2}	80	3.2	+560		1.7×10^{18}	0.23	83

International Journal of Innovative Research in Science, Engineering and Technology

(An ISO 3297: 2007 Certified Organization)

Website: www.ijirset.com

Vol. 6, Issue 2, February 2017

VI. CONCLUSION

In this review properties and applications of oxide materials has been discussed. In our daily life, transparent conducting oxide materials are used in numerous devices. These applications are mostly found in display technology, OLEDs, thin-film solar photovoltaics, smart windows and solid state gas sensors. Electronic and optical properties of TCOs have been discussed. Particular deposition techniques for TCO's manufacturing are chosen for several reasons as thickness uniformity and low production costs. However, the electrical and optical performance is not directly related to the deposition methods. They are more dependent on the intrinsic properties as structure, surface morphology and composition of the thin film. Each deposition method and ambient conditions can influence the intrinsic behaviour differently.

REFERENCES

- [1] J.P. Colinge, K. Hashimoto, T. Kamins, S.Y. Chiang, E.D. Liu, S.S. Peng, and P. Rissman, "High-speed, low-power, implanted-buried-oxide CMOS circuits", IEEE Electron Device Lett., vol. 7, pp. 279-281, 1986.
- [2] V. Srinivasan, and J.W. Weidner, "An Electrochemical route for making porous nickel oxide electrochemical capacitors", J. Electrochem. Soc., vol. 144, pp. 210-213, 1997.
- [3] B.C. Yadav, R. Singh, and S. Singh, "Investigations on humidity sensing of nanostructured tin oxide synthesised via mechanochemical method", J. Experimental Nanoscience, vol.5, pp. 1-14, 2012.
- [4] S. Singh, A. Singh, M. Wan, R.R. Yadav, P. Tandon, S.S.A. Rasool, B.C. Yadav, "Fabrication of self-assembled hierarchical flowerlike zinc stannate thin film and its application as liquefied petroleum gas sensor" Sens. Actuators B: Chem. vol. 205, pp. 102-110, 2014.
- [5] R.K. Sonker, A. Sharma, M. Tomar, B.C. Yadav, and V. Gupta, "Nanocatalyst (Pt, Ag and CuO) Doped SnO₂ Thin Film Based Sensors for Low-Temperature Detection of NO₂ Gas", Adv. Sci. Lett. vol. 20, pp. 1374-1377, 2014.
- [6] R. Singh, S. Singh, R. Srivastava, A. Mishra, and B.C. Yadav, "Humidity Sensing Investigations on Nanostructured Antimony-Substituted Tin Oxide Nanoparticles", Adv. Sci. Lett. vol. 20, pp. 887-894, 2014.
- [7] R. Singh, and B. C. Yadav, "Synthesis and Characterization of Copper Doped Tin Oxide for Humidity Sensing Applications", Adv. Sci. Lett. vol. 20, pp. 895-902, 2014.
- [8] R.K. Sonker, A. Sharma, M. Tomar, V. Gupta, and B.C. Yadav, "Low-Temperature Operated NO₂ Gas Sensor Based on SnO₂-ZnO Nanocomposite Thin Film", Adv. Sci. Lett. vol. 20, pp. 911-916, 2014.
- [9] R.K. Sonker, and B.C. Yadav, "Chemical Route Deposited SnO₂, SnO₂-Pt and SnO₂-Pd Thin Films for LPG Detection", Adv. Sci. Lett. vol. 20, pp. 1023-1027, 2014.
- [10] S. Singh, N. Verma, A. Singh, B.C. Yadav, "Synthesis and characterization of CuO-SnO₂ nanocomposite and its application as liquefied petroleum gas sensor", Mater. Sci. in Semiconductor Processing, vol. 18, no. C, pp. 88-96, 2014.
- [11] B.C. Yadav, P. Sharma, P.K. Khanna, "Morphological and Humidity Sensing Characteristics of SnO₂-CuO, SnO₂-Fe₂O₃ and SnO₂-SbO₂ nano co-oxides", Bull. of Mater. Sci., vol. 34, no. 1, pp. 1-10, 2011.
- [12] B.C. Yadav, S. Sikarwar, A. Bhaduri, and P. Kumar, "Synthesis, Characterization and Development of Opto-Electronic Humidity Sensor using Copper Oxide Thin Film", Int. Adv. Res. J. in Sci., Engg and Tech. vol. 2, no. 11, pp. 105-109, 2015.
- [13] B. Noheda, "Structure and high-piezoelectricity in lead oxide solid solutions", Curr. Opin. Solid-State Mater. Sci., vol. 6, pp. 27-34, 2002.
- [14] K. Eguchi, T. Setoguchi, T. Inoue, and H. Arai, "Electrical properties of ceria-based oxides and their application to solid oxide fuel cells", Solid State Ionics, vol. 52, pp. 165-172, 1992.
- [15] C.C. Hsu, and N.L. Wu, "Synthesis and photocatalytic activity of ZnO/ZnO₂ composite" J. Photochem. Photobiol. A, vol. 172, pp. 269-274, 2005.
- [16] S. Lindroos, and M. Leskela, "The growth of zinc peroxide (ZnO₂) and zinc oxide (ZnO) thin films by the successive ionic layer adsorption and reaction - SILAR - technique", Int. J. Inorg. Mater. vol. 2, pp. 197-201, 2000.
- [17] D. Golberg, Y. Bando, K. Fushimi, M. Mitome, L. Bourgeois, and C.C. Tang, "Nanoscale oxygen generators: MgO₂ fillings of BN nanotubes, J. Phys. Chem. B, vol. 107, pp. 8726-8729, 2003.
- [18] A. Wada, F. Wang, Y. Suhara, Y. Yamano, T. Okitsu, K. Nakagawa, and T. Okano, "Efficient synthesis and biological evaluation of dimethylgeranylgeranoic acid derivatives", Bioorg. Med. Chem. vol. 18, pp. 5795-5806, 2010.
- [19] T. Okitsu, D. Nakazawa, K. Nakagawa, T. Okano, and A. Wada, "Synthesis and biological evaluation of 9Z-retinoic acid analogues having 2-substituted benzofuran", Chem. Pharm. Bull. vol. 58, pp. 418-422, 2010.
- [20] K. Nakagawa, J. Sugita, and K. Igano, "Oxidation with nickel peroxide. 3. oxidative cleavage of alpha-glycols, alpha-hydroxy acids, alpha-keto alcohols, and alpha-keto acids", Chem. Pharm. Bull. vol. 12, pp. 403-409, 1964.
- [21] K. Nakagawa, J. Sugita, and H. Onoue, "Oxidation with nickel peroxide. iv. The preparation of benzoxazoles from Schiff's bases", Chem. Pharm. Bull. vol. 12, pp. 1135-1142, 1964.
- [22] C. Pierlot, V. Nardello, J. Schrive, C. Mabile, J. Barbillat, B. Sombret, and J.M. Aubry, "Calcium peroxide diperoxhydrate as a storable chemical generator of singlet oxygen for organic synthesis", J. Org. Chem. vol. 67, pp. 2418-2423, 2002.

International Journal of Innovative Research in Science, Engineering and Technology

(An ISO 3297: 2007 Certified Organization)

Website: www.ijirset.com

Vol. 6, Issue 2, February 2017

- [23] C.G. Levi, J.Y. Yang, B.J. Dalgleish, F.W. Zok, and A.G. Evans, "Processing and performance of an all-oxide ceramic composite", *J. Am. Ceram. Soc.* vol. 81, pp. 2077-2086, 1998.
- [24] A. Nazeri, P.P. Trzaskoma, Paulette, and D. Bauer, "Synthesis and properties of cerium and titanium oxide thin coatings for corrosion protection of 304 stainless steel", *J. Sol-Gel Sci. Technol.* Vol. 10, pp. 317-331, 1997.
- [25] Z.R. Tian, W. Tong, J.Y. Wang, N.G. Duan, V.V. Krishnan, and S.L. Suib, "Manganese oxide mesoporous structures: mixed-valent semiconducting catalysts", *Science.* vol. 276, pp. 926-929, 1997.
- [26] I.E. Wachs, "Raman and IR studies of surface metal oxide species on oxide support: supported metal oxide catalysts", *Catal. Today*, vol. 27, pp. 437-455, 1996.
- [27] G.C. Bond, and S.F. Tahir, "Vanadium oxide monolayer catalysts Preparation, characterization and catalytic activity", *Appl. Catal.*, vol. 71, pp. 1-31, 1991.
- [28] A.H. Wilson, "The theory of electronic semiconductors", *Proc. Roy. Soc. A*, vol. 133, pp. 458-491, 1931.
- [29] Z.L. Wang, "Functional oxide nanobelts: materials, properties and potential applications in nanosystems and biotechnology", *Annu. Rev. Phys. Chem.* vol. 55, pp. 159-196, 2004.
- [30] M.F. Garcia, A.M. Arias, J.C. Hanson, and J.A. Rodriguez, "Nanostructured oxides in chemistry: characterization and properties", *Chem. Rev.* vol. 104, pp. 4063-4104, 2004.
- [31] M.E. Franke, T.J. Koplin, and U. Simon, "Metal and metal oxide nanoparticles in chemiresistors: does the nanoscale matter", *Small.* vol. 2, pp. 36-50, 2006.
- [32] S. Sikarwar, B.C. Yadav, S. Singh, G.I. Dzhardimalieva, S.I. Pomogailo, N.D. Golubeva, A.D. Pomogailo, "Fabrication of nanostructured yttrium-stabilized zirconia multilayered films and their optical humidity sensing capabilities based on transmission", *Sens. Actuators B: Chem.* vol. 232, pp. 283-291, 2016.
- [33] F. Zhu, Z.X. Yang, W.M. Zhou, and Y.F. Zhang, "Direct synthesis of beta gallium oxide nanowires, nanobelts, nanosheets and nano grasses by microwave plasma", *Solid State Commun.* vol. 137, pp. 177-181, 2006.
- [34] W.J. Lee, and W.H. Smyrl, "Zirconium oxide nanotubes synthesised via direct electrochemical anodization", *Electrochem*, *Solid-State Lett.*, vol. 8, pp. B7-B9, 2005.
- [35] K. Deshpande, A. Mukasyan and A. Varma, "Direct synthesis of iron oxide nanopowders by the combustion approach: reaction mechanism and properties", *Chem. Mater.*, vol. 16, pp. 4896-4904, 2004.
- [36] H.Y. Dang, J. Wang, and S.S. Fan, "The synthesis of metal oxide nanowires by directly heating samples in appropriate oxygen atmospheres", *Nanotechnology.* vol. 14, pp. 738-741, 2003.
- [37] M. Kakihana, "Sol-gel preparation of high-temperature superconducting oxides", *J. Sol-Gel Sci. Technol.* vol. 6, pp. 7-55, 1996.
- [38] M. Niederberger, and G. Garnweitner, "Organic Reaction Pathways in the Nonaqueous Synthesis of Metal Oxide Nanoparticles", *Chem. Eur. J.* vol. 12, pp. 7282-7302, 2006.
- [39] A.P. Alivisatos, "Semiconductor clusters, nanocrystals, and quantum dots", *Science*, vol. 271, pp. 933-937, 1996.
- [40] C.G. Granqvist, and A. Hultaker, "Transparent and conducting ITO films: new developments and applications", *Thin Solid films.* vol. 411, pp. 1, 2002.
- [41] R. Groth, and E. Kauer, "Thermal Insulation of Sodium Lamps", *Philips Technical Review.* vol. 26, pp. 105, 1965.
- [42] H. Ohta, K.I. Kawamura, M. Orita, M. Hirano, N. Sarukura, and H. Hosono, "Current injection emission from a transparent p-n junction composed of p-SrCu₂O₂/n-ZnO", *Appl. Phys. Lett.* vol. 77, pp. 475-477, 2000.
- [43] K. Tonooka, H. Bando, and Y. Aiura, "Photovoltaic effect observed in transparent p-n heterojunctions based on oxide semiconductors", *Thin Solid Films.* vol. 445, pp. 327-331, 2003.
- [44] H. Hosono, H. Ohta, K. Hayashi, M. Orita, and M. Hirano, "Near-UV emitting diodes based on a transparent p-n junction composed of heteroepitaxially grown p-SrCu₂O₂ and n-ZnO", *J. Cryst. Growth.* vol. 237, pp. 496-502, 2002.
- [45] R.E. Presley, D. Hong, H.Q. Chiang, C.M. Hung, R.L. Hoffman, and J.F. Wager, "Transparent ring oscillator based on indium gallium oxide thin-film transistors", *Solid-State Electron.* vol. 50, pp. 500, 2006.
- [46] H. Kawazoe, H. Yanagi, K. Ueda, and H. Hosono, "Transparent p-type conducting oxides: design and fabrication of p-n heterojunctions", *MRS Bull.*, vol. 25, pp. 28-36, 2000.
- [47] K.L. Chopra, S. Major, and D.K. Pandya, "Transparent conductors-A status review", *Thin Solid Films*, vol. 102, pp. 1-46, 1983.
- [48] N.F. Mott, "On the Transition to Metallic Conduction in Semiconductors", *Can. J. Phys.* vol. 34, pp. 1356-1368, 1956.
- [49] I. Hamberg, and C.G. Granqvist, "Evaporated Sn-doped In₂O₃ films: basic optical properties and applications to energy-efficient windows", *J. Appl. Phys.* vol. 60, pp. R123-R160, 1986.
- [50] J.S. Blakemore, "Semiconducting and other major properties of gallium arsenide", *J. Appl. Phys.* vol. 53, pp. R123-R181, 1982.
- [51] M. Chen, Z.L. Pei, X. Wang, Y.H. Yu, X.H. Liu, C. Sun, and L.S. Wen, "Intrinsic limit of electrical properties of transparent conductive oxide films", *J. Phys. D: Appl. Phys.* vol. 33, pp. 2538-2548, 2000.
- [52] E.J. Moore, "Quantum-transport theories and multiple scattering in doped semiconductors. II. The mobility of n-type gallium arsenide", *Phys. Rev.* vol. 160, pp. 618-626, 1967.
- [53] T. Pisarkiewicz, K. Zakrzewska, and E. Leja, "Scattering of charge carriers in transparent and conducting thin oxide films with a non-parabolic conduction band", *Thin Solid Films.* vol. 174, pp. 217-223, 1989.
- [54] J.Y.W. Seto, "The electrical properties of polycrystalline silicon films", *J. Appl. Phys.* vol. 46, pp. 5247-5254, 1975.
- [55] R.L. Petritz, "Theory of photoconductivity in semiconductor films", *Phys. Rev.* vol. 104, pp. 1508-1516, 1956.
- [56] J. Bruneaux, H. Cachet, M. Froment, and A. Messad, "Correlation between structural and electrical properties of sprayed tin oxide films with and without fluorine doping", *Thin Solid Films.* vol. 197, pp. 129-142, 1991.

International Journal of Innovative Research in Science, Engineering and Technology

(An ISO 3297: 2007 Certified Organization)

Website: www.ijirset.com

Vol. 6, Issue 2, February 2017

- [57] K. Ellmer, "Resistivity of polycrystalline zinc oxide films: current status and physical limit", J. Phys. D: Appl. Phys. vol. 34, pp. 3097-3108, 2001.
- [58] C. Erginsoy, "Neutral impurity scattering in semiconductors", Phys. Rev. vol. 79, pp. 1013-1014, 1950.
- [59] S. Noguchi, and H. Sakata, "Electrical properties of Sn-doped In_2O_3 prepared by reactive evaporation", J. Phys. D: Appl. Phys. vol. 14, pp. 1523-1530, 1981.
- [60] J.C. Manificier, M.D. Murcia, J.P. Fillard, and E. Vicario, "Optical and electrical properties of SnO_2 thin films in relation to their stoichiometric deviation and their crystalline structure", Thin Solid Films, vol. 41, pp. 127-135, 1977.
- [61] R.T. Chen, and D. Robinson, "Electro-optic and all-optical phase modulator on an indium tin oxide single-mode waveguide", Appl. Phys. Lett., vol. 60, pp. 1541-1544, 1992.
- [62] Y. Ohhata, F. Shinoki, and S. Yoshida, "Optical properties of r.f. reactive sputtered tin-doped In_2O_3 films", Thin Solid Films, vol. 59, pp. 255-261, 1979.
- [63] A. De and, S. Ray, "A study of the structural and electronic properties of magnetron sputtered tin oxide films", J. Phys. D: Appl. Phys. vol. 24, pp. 719-726, 1991.
- [64] E. Santhani, A. Banerjee, V. Dutta, and K.L. Chopra, "Electrical and optical properties of tin oxide films doped with F and (Sb+F)", J. Appl. Phys. vol. 53, pp. 1615-1621, 1982.
- [65] V. Casey, and M.I. Stephenson, "A study of undoped and molybdenum doped, polycrystalline, tin oxide thin films produced by a simple reactive evaporation technique", J. Phys. D: Appl. Phys. vol. 23, pp. 1212-1215, 1990.
- [66] S. Gupta, B.C. Yadav, P.K. Dwivedi, and B. Das, "Microstructural, optical and electrical investigations of Sb- SnO_2 thin films deposited by spray pyrolysis", Mater. Res. Bull. vol. 48, pp. 3315-3322, 2013.
- [67] S. Schiller, G. Beister, E. Buedke, H.J. Becker, and H. Schicht, "Properties of cadmium stannate thin films produced by reactive high rate d.c. magnetron-plasmatron sputtering", Thin Solid Films, vol. 96, pp. 113-120, 1982.
- [68] T. Minami, T. Kakumu, K. Shimokawa, and S. Takata, "New transparent conducting $\text{ZnO-In}_2\text{O}_3\text{-SnO}_2$ thin films prepared by magnetron sputtering", Thin Solid Films. vol. 317, pp. 318-321, 1998.
- [69] J.M. Phillips, J. Kwo, G.A. Thomas, S.A. Carter, R.J. Cava, S.Y. Hou, J.J. Krajewski, J.H. Marshall, W.F. Peck, D.H. Rapkine, and R.D. van Dover, "Transparent conducting thin films of GaInO_3 ", Appl. Phys. Lett. vol. 65, pp. 115-117, 1994.
- [70] S.A. Agnihotry, K.K. Saini, T.K. Saxena, K.C. Nappal, and S. Chandra, "Studies on e-beam deposited transparent conductive films of $\text{In}_2\text{O}_3\text{:Sn}$ at moderate substrate temperatures", J. Phys. D: Appl. Phys. vol. 18, pp. 2087-2098, 1985.
- [71] T. Maruyama, and K. Fukui, "Indium-tin oxide thin films prepared by chemical vapour deposition", J. Appl. Phys. vol. 70, pp. 3848-3851, 1991.
- [72] K. Sreenivas, T.S. Rao, and A. Mansingh, "Preparation and characterization of rf sputtered indium tin oxide films", J. Appl. Phys. vol. 57, pp. 384-392, 1985.
- [73] C. Geoffroy, G. Campet, J. Portier, J. Salardenne, G. Couturier, M. Bourrel, J.M. Chabagno, D. Ferry, and C. Quet, "Preparation and characterization of fluorinated indium tin oxide films prepared by r.f. sputtering", Thin Solid Films. vol. 202, pp. 77-82, 1991.
- [74] J.B. Webb, D.F. Williams, and M. Buchanan, "Transparent and highly conductive films of ZnO prepared by rf reactive magnetron sputtering", Appl. Phys. Lett. vol. 39, pp. 640-642, 1981.
- [75] J. Hu, and R.G. Gordon, "Textured aluminum-doped zinc oxide thin films from atmospheric pressure chemical-vapor deposition", J. Appl. Phys. vol. 71, pp. 880-890, 1991.
- [76] B.H. Choi, H.B. Im, J.S. Song, and K.H. Yoon, "Optical and electrical properties of Ga_2O_3 -doped ZnO films prepared by r.f. sputtering, Thin Solid Films. vol. 193-194, pp. 712-720, 1990.
- [77] A. Sarkar, S. Ghosh, S. Chaudhuri, and A.K. Pal, "Studies on electron transport properties and the Burstein-Moss shift in indium-doped ZnO films", Thin Solid Films. vol. 204, pp. 255-264, 1991.
- [78] N. Naghavi, A. Rougier, C. Marcel, C. Guéry, J.B. Leriche, and J.M. Tarascon, "Characterization of indium zinc oxide thin films prepared by pulsed laser deposition using a $\text{Zn}_3\text{In}_2\text{O}_6$ target", Thin Solid Films. vol. 360, pp. 233-240, 2000.
- [79] H. Yanagi, S.I. Inoue, K. Ueda, H. Kawazoe, H. Hosono, and N. Hamada, "Electronic structure and optoelectronic properties of transparent p-type conducting CuAlO_2 ", J. Appl. Phys. vol. 88, pp. 4159-4163, 2000.
- [80] A. Kudo, H. Yanagi, H. Hosono, and H. Kawazoe, "Sr Cu_2O_2 : A p-type conductive oxide with a wide band gap", Appl. Phys. Lett. vol. 73, pp. 220-222, 1998.
- [81] M.K. Jayaraj, A.D. Draeseke, J. Tate, and A.W. Sleight, "p-type transparent thin films of $\text{CuY}_{1-x}\text{Ca}_x\text{O}_2$ ", Thin Solid Films, vol. 397, pp. 244-248, 2001.
- [82] J. Tate, M.K. Jayaraj, A.D. Draeseke, T. Ulbrich, A.W. Sleight, K.A. Vanaja, R. Nagarajan, J.F. Wager, and R.L. Hoffman, "p-type oxides for use in transparent diodes", Thin Solid Films, vol. 411, pp. 119-124, 2002.
- [83] K. Ueda, T. Hase, H. Yanagi, H. Kawazoe, H. Hosono, H. Ohta, M. Orita, and M. Hirano, "Epitaxial growth of transparent p-type conducting CuGaO_2 thin films on sapphire (001) substrates by pulsed laser deposition", J. Appl. Phys. vol. 89, pp. 1790-1793, 2001.